Batle et al. *EPJ Quantum Technology* (2024) 11:62
https://doi.org/10.1140/epjqt/s40507-024-00273-7

EPJ Quantum Technology
a SpringerOpen Journal

EPJ.org

RESEARCH Open Access

Quantum null-hypothesis device-independent Schmidt number witness

Josep Batle[1,2], Tomasz Białecki[3], Tomasz Rybotycki[4,5,6], Jakub Tworzydło[3] and Adam Bednorz[3*]

*Correspondence:
Adam.Bednorz@fuw.edu.pl
[3]Faculty of Physics, University of Warsaw, ul. Pasteura 5, PL02-093 Warsaw, Poland
Full list of author information is available at the end of the article

Abstract

We investigate the dimensionality of bipartite quantum systems by construction of a device-independent null witness test. This test assesses whether a given bipartite state conforms with the expected quantum dimension, Schmidt number, and distinguishes between real and complex spaces. By employing local measurements on each party, the proposed method aims to determine the minimal rank. By performing an experimental demonstration on IBM Quantum devices, we prove the exceptional accuracy of the test and its usefulness in diagnostics beyond routine calibrations. One of the tests shows agreement with theoretical expectations within statistical errors. However, the second test failed by more than 6 standard deviations, indicating unspecified parasitic entanglements, with no known simple origin.

Keywords: Quantum dimension; Entanglement; Null witness

1 Introduction

Quantum bipartite systems differ from their classical counterparts, especially when entangled. They violate local realism [1–5] and are useful in quantum computation, steering and teleportation [6–9]. The most common Bell entangled state involves both two-level parties. In this case, correlations can be predicted from the knowledge of the state and available measurements.

On the other hand, it is important to assess the dimension of the system in question (quantum or classical) for the error correction and mitigation tools to work, assuming restricted Hilbert spaces [10–12]. So far, such tests involved a single party, when a protocol of independent sets of preparations and measurements allowed construction of a dimension witness, initially in the form of inequalities [13, 14], also tested experimentally [15–18]. Analogous tests, as inequalities, have been proposed for bipartite states [19–23] based on families of Bell-type inequalities [24]. If the contribution from extra states is small it is better to seek a null test (a function of probabilities is exactly equal to zero), for instance the Sorkin identity [25] in the three-slit experiment [26–28] verifying Born's rule [29] under certain assumptions. The quantum dimension can also be tested by null

Springer

hypotheses [30–32], demonstrated experimentally [33, 34]. Testing an exact value, up to statistical error, boosts the accuracy of the test.

In this work, we propose the test if a bipartite state is of the expected quantum dimension as a null hypothesis, based on independent measurements of each party, i.e. a measurement-measurement scenario with a single, common preparation, in contrast to the previous preparation-measurement protocol [30, 33]. We construct a witness, function of bipartite probabilities, which is zero if any party can be represented in the space of the expected dimension, depending on whether the space is complex or real [35]. The measurements can be arbitrary, device-independent, but must be performed in local subspaces. In other words, we test the *minimal* bipartite space dimension to represent the state, called Schmidt number [36, 37]. Existing witnesses of the Schmidt number [38–48] are based on inequalities, often only state-independent, or only narrowly violated in a larger space. Note that, like Bell-type test, any violation requires nonclassical states for linear inequalities, and quite faithful implementation of quantum operations on physical devices. Therefore, linear inequalities, although robust against calibration changes, are in principle less accurate and less general than null witnesses, as Schmidt number is independent of nonclassicality. Then the larger dimension is usually already clear by the implementation itself. On the other hand, a null device-independent witness is useful when the space is trusted to be restricted and one has no access to accurate operations, which can be noisy. It is a precise tool to certify the device solely with respect to its Hilbert dimension, not errors within the space.

Our witness tests if an entangled state has the expected Schmidt number d by (a) n measurements chosen by each of the two parties or (b) single measurements with $n+1$ outcomes. The measured observables can be arbitrary and their representation is irrelevant as long as they are local. The witness is the determinant of the probability matrix [49], of size depending on the dimension, becoming 0 for sufficiently large n, up to a finite statistics error. Moreover, we demonstrate the feasibility of the test on qubits on IBM Quantum, if a created entangled state fits in the 2×2 qubit-qubit bipartite space. The results of the test (a) are in agreement with the null hypothesis within the corresponding statistical errors. The locality of measurements implies that the parties cannot affect each other, so one can perform simultaneously the sanity check of no-signaling, common also in experimental Bell-type tests [50–53]. However, the test (b) failed by more than 6 standard deviations. Taking into account the robustness of our test against local errors and negligible leakage and crosstalk contribution, it shows extreme accuracy of our test, revealing problems beyond standard diagnostics, which demand urgent explanation, either technical or fundamental.

2 The witness

Suppose we have a composite (tensor) system of A and B and the initially prepared state $\rho = \mathcal{E}_A \mathcal{E}_B \tilde{\rho}$, where $\mathcal{E}$ are local maps in respective subspaces [54]. To shorten notation, we shall drop the tensor sign whenever unambiguous, i.e. $\mathcal{E}_A \mathcal{E}_B \equiv \mathcal{E}_A \otimes \mathcal{E}_B$ and $AB \equiv A \otimes B$. Assuming the form

$$\rho = \sum_k |\psi_k\rangle\langle\psi_k| \tag{1}$$

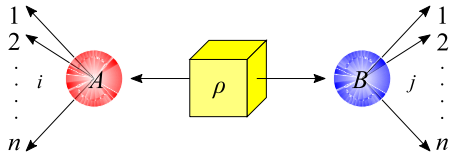

Figure 1 Two parties A and B perform either (a) one of n independent measurements indexed by i and j or (b) single measurements with n outcomes, also indexed by i and j, on the shared bipartite states ρ. The case (b) differs from (a) by imposed condition that outcomes sum up to identity measurement

with states $|\psi_k\rangle$, we can purify $\tilde{\rho}$ by adding the auxiliary system C, so that $\tilde{\rho} = |\psi\rangle\langle\psi|$ with $|\psi\rangle = \sum_k |\psi_k, k\rangle$, so that k labels the basis states in C. The Schmidt number [36, 37] is the minimal possible number d of basis states in the Schmidt decomposition in the respective spaces A and BC,

$$|\psi\rangle = \sum_{k'=1}^{d} |k'_A k'_{BC}\rangle. \tag{2}$$

In the above purification $\mathcal{E}_A$ is the identity, while $\mathcal{E}_B = \mathrm{Tr}_C$ (tracing out C).

We define the probability

$$p_{ij} = \mathrm{Tr}\, A_i B_j \rho = \langle\psi|\tilde{A}_i \tilde{B}_j|\psi\rangle, \tag{3}$$

with $\tilde{A}_i = \mathcal{E}_A^\dagger A_i$, $\tilde{B}_j = \mathcal{E}_B^\dagger B_j$ for the observables A_i, B_j and local maps $\mathcal{E}_A$, $\mathcal{E}_B$ for the above constructed Schmidt decomposition states $|\psi\rangle$. Replacing $\tilde{A}_i \to A_i$, $\tilde{B}_j \to B_j$, and $|\psi\rangle\langle\psi| \to \rho$, we can reduce the whole discussion of the Schmidt number to the $d \times d$ dimensional composite Hilbert space. Let us construct lists of local Hermitian observables (a) $0 \le A_i, B_j \le 1$ for $i, j = 1 \ldots n$ with yes/no or 1/0 outcome for n independent measurements and auxiliary $A_0 = B_0 = 1$, or (b) $0 \le A_i, B_j$ for $i, j = 1 \ldots n+1$ and $\sum_i A_i = \sum_i B_i = 1$ for single measurements with $n+1$ outcomes, see Fig. 1. In the case (a) the actual number of measurements is $n \times n$. Then the first row and column (0) do not need a separate measurement, as one can simply discard the outcome of the other party from measurements already done. Nevertheless, these entries must satisfy no-signaling (independence of the measurement on the other party), i.e. p_{i0} (or p_{0j}) is obtained in the measurement (i, j) but cannot depend on j (or i). The corner element is constant $p_{00} = 1$. In both cases, our witness is the $(n+1) \times (n+1)$ determinant $W_n = \det p$ which is equal 0 if the Schmidt number satisfies $d^2 \le n$ (complex space) or $d(d+1)/2 \le n$ (real space) because the size of p exceeds the maximal rank of the set of allowed matrices A_i or B_j, which span the available linear space. If the dimension of the linear space of observables is smaller than the size of the matrix then some observable must be a linear combination of the rest. By linearity of the matrix (3) as a function of observables, the same applies to its corresponding column or row, and the determinant must vanish. The real symmetric matrix $d \times d$ is represented by $d(d+1)/2$ independent real numbers. A complex Hermitian matrix has additionally $d(d-1)/2$ real independent numbers representing imaginary antisymmetric matrices. The test is device-independent, we make no assumption about the actual realization of measurements, that is the test does not rely on the mathematical model of the observables.

This happens in the case $d = 2$ real for $n \ge 3$, and $d = 2$ complex for $n \ge 4$ which is the case we test. For instance, if $W_4 \ne 0$ then either we have (i) a quantum system of $d = 3$ or (ii) a classical system of $d = 5$. This is why our test is not intended to check just whether

the system is classical or quantum but rather the value of d, depending on the type of the system.

Even if the Schmidt number is larger than expected, the witness can remain zero by accident. Nevertheless, the absolute upper bound on W_n, the same in the classical and quantum case (see detailed proof in Appendix A), allows us to estimate how large the witness can be if the expected d is exceeded. To determine it over possible states and measurements, let us consider a simpler, classical case. Suppose the composite system has the states (i',j') for the parties A and B, $i',j' = 1\dots d$. Then the probability reads

$$p_{ij} = \sum_{i'j'} A_{ii'}\rho_{i'j'}B_{j'j} \tag{4}$$

where ρ_{rs} is the probability distribution of the systems, $\rho_{i'j'} \geq 0$, $\sum_{i'j'}\rho_{i'j'} = 1$, $A_{ii'} \in [0,1]$ is the probability to read 1 from i' in the measurement $i \geq 1$ ($A_{0i'} = 1$ in the case (a)), and analogously $B_{j'j}$. By linearity of the determinant with respect to rows/columns and Cauchy-Binet formula, the upper bound turns out to be 4^{-n} in the case (a). In the case (b), the determinant is the product of eigenvalues whose sum is bounded by trace, and the trace is bounded by 1 (sum of all probabilities), so by arithmetic and geometric means the maximum is $(n+1)^{-n-1}$, saturated whenever $d > n$, taking $\rho_{i'} = 1/(n+1)$ for $i' = 1\dots n+1$ and $A_{ii'} = B_{i'i} = \delta_{ii'}$.

For the limited d in the case (a), the classical extremal cases have been tabularized in Table 1. In the quantum case of (a), we reach the bound for $n = 1,2$ for $d = 2$, in the real case, and $n = 3$ for $d = 2$ in the complex case. For $d = 4$ the upper bound $W_n = 4^{-n}$ is reached for $n \leq 9$ and $n \leq 15$ in the real and complex cases, respectively. The result for $d = 4$ (ququarts) is obtained as follows. We take two qubits for each party to span $d = 4$ space. We use the maximally entangled state $|\psi\rangle = \sum_x |x,x\rangle/2$ with $x = 00, 01, 10, 11$ in this space for a single party. In such a case, the probabilities from (3) read

$$p_{ij} = \sum_{xy}\langle x,x|A_iB_j|y,y\rangle/2 = \sum_{xy}(A_i)_{xy}(B_j)_{xy}/4 = \mathrm{Tr}\,A_iB_j^*/4, \tag{5}$$

i.e. a direct matrix product (not tensor) for A_i and B_j written in the basis $|x\rangle$, according to (3). Here the observables are represented by $A_{st} = B_{st}^* = (1+\sigma_s^1\sigma_t^2)/2$ with the upper index denoting the qubit, and $st = 0,1,2,3$ denoting the standard Pauli matrices. It is clear that any subset of such observables built for pairs (st) (with $st = 0,1,3$ except $s = t = 0$) will maximize W because of mutual orthogonality in terms of Hilbert-Schmidt scalar product $\mathrm{Tr}\,XY^\dagger$. All observables from the set are real, plus one extra for $s = t = 2$. We then get the

Table 1 The calculated maxima for the test (a) of the witness quantity 4^nW_n in the classical approach for $d = 2\dots 8$ and number of measurements $n = 1\dots 5$. Entries in the empty cells saturate the bound at 1

$n\backslash d$	2	3	4	5	6	7	8
1	1						
2	0	0.59	1				
3	0	0	1				
4	0	0	0	0.74	0.76	0.79	1
5	0	0	0	0	0.55	0.59	1

Table 2 The calculated fully quantum maxima for the test (a) of the witness quantity $4^n W_n$ for $d = 2(r/c), 3(r/c)$ with (r/c) denoting the real/complex case

$n\backslash d$	$2r$	$2c$	$3r$	$3c$
1	1	1	1	1
2	1	1	1	1
3	0	1	0.85	1
4	0	0	0.55	0.78
5	0	0	0.38	0.69
6	0	0	0	0.54
7	0	0	0	0.35
8	0	0	0	0.25

upper bound for real ququarts up to $n \leq 9$. In the complex case, to get the upper bound, we can take all possible (st) except (00) up to $n \leq 15$. For lower d we determined the bounds of W numerically and collected the results in Table 2 (see details in Appendix B).

In the case (b), the maximum is classical for $d > n$. For $d \leq n$ the total maximum is $[(d-1)/n]^n/(n+1)^{n+1}$, saturated for maximally entangled states and single projection observables $A_i = B_i$ equal single projections corresponding to equiangular tight frames [55] times a constant, see details in Appendix A. In cases without equiangular tight frames, one has to determine the maxima numerically. For $n < 5$, the only such cases are $n = 4$, $d = 3$ real $1.6875 \cdot 10^{-5}$ and complex $1.8746 \cdot 10^{-5}$, lower than the equiangular bound $2 \cdot 10^{-5}$, see details in Appendix B.

We also stress that the naive application of a preparation and measurement scenario [33] cannot verify per se the Schmidt number in the bipartite case because of the nonlinearity of the product states (we present a counterexample in Appendix C).

3 Error analysis

To determine the value of the witness W_n, we collect data from N repetitions of each measurement combination. The uncertainty in determining W_n is analogous to the prepare-measure scheme in Ref. [32] for finite statistics and assuming $\langle W_n \rangle = 0$. In our notation, the resulting error, $N\Delta W_n^2$, is

$$\begin{aligned} &\sum_{kj} \mathcal{A}_{jk}^2 p_{kj}(1-p_{kj}) && \text{case (a)}, \\ &\sum_{kj} \mathcal{A}_{jk}^2 p_{kj} - \left(\sum_{kj} \mathcal{A}_{jk} p_{kj}\right)^2 && \text{case (b)}, \end{aligned} \tag{6}$$

with the adjugate matrix $\mathcal{A} = \mathrm{Adj}\, p$ calculated directly, since $p^{-1} \det p$ does not exist when $\det p = 0$. One should also avoid the situation of $\mathcal{A} = 0$, i.e. when the rank is already smaller, as the error becomes not reliable, and one has to consider second-order minors. In our measure-measure approach, in the case (a), the no-signaling assumption means that, in principle, the probabilities p_{0j} and p_{k0} are not independently measured. The simplest approach is to take them averaged from other experiments, while still treating them as independent. In this way, we just find an upper estimate for the error. On the other hand, verifying no-signaling is an important sanity check, which we perform in Appendix D.

4 Demonstration on IBM Quantum

We have demonstrated the feasibility of the above test on IBM Quantum devices. A microwave pulse tuned to the interlevel drive frequency allows one to apply the parametrically controlled gates. The native single qubit gate is the $\pi/2$ rotation

$$S = \sqrt{-iX} = (\sigma_0 - i\sigma_1)/\sqrt{2}, \tag{7}$$

in the $|0\rangle$, $|1\rangle$ basis. The rotation for a given angle θ is realized with the native gate S and two gates Z_θ

$$S_\theta = Z_\theta^\dagger S Z_\theta, Z_\theta = \sigma_0 \cos\theta/2 - i\sigma_3 \sin\theta/2, \tag{8}$$

with shorthand notation $Z = iZ_\pi$, $Z_\pm = Z_{\pm\pi/2}$. In addition, there is a native two-qubit *CNOT* gate on most of IBM quantum devices, operating as

$$|00\rangle\langle 00| + |01\rangle\langle 01| + |11\rangle\langle 10| + |10\rangle\langle 11|, \tag{9}$$

where for $|ab\rangle$ the control qubit state is a (depicted as $\bullet$) and target qubit state is b (depicted as $\oplus$ in Fig. 2). The newest devices use Echoed Crossed Resonance (*ECR*) gate, instead of *CNOT* but one can transpile the latter by additional single-qubits gates, see Appendix E.

In the case (a), we create the Bell state $(|+-\rangle - |-+\rangle)/\sqrt{2}$ with 2 or 3 qubits between A and B, where $|+\rangle = |0\rangle$, $|-\rangle = |1\rangle$ for A and $|+\rangle = i|1\rangle$, $|-\rangle = |0\rangle$ for B. The final measurement is fixed by two subsequent local gates $S_{1,2}$ from (8), with appropriately chosen angles θ_1, θ_2 as explained below. We took two different sets of measurements: set I and set II. In the language of the Bloch sphere, our measurement directions are eigenstates of $\vec{a}\cdot\vec{\sigma}$ with the eigenvalue +1 for a unit vector $\vec{a}$. We took four vectors for A and the opposite vectors

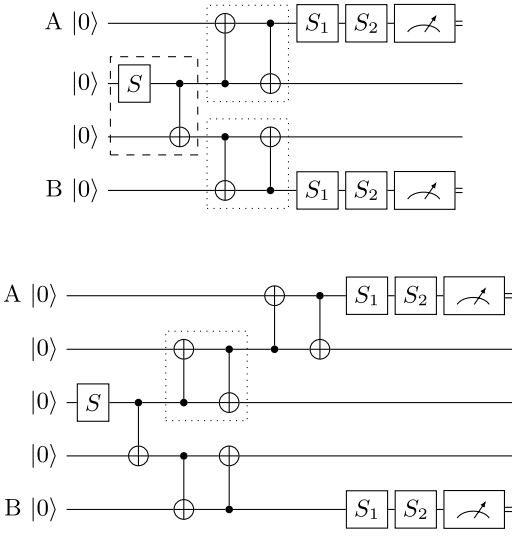

Figure 2 The implementation of the test (a) on IBM Quantum with two (top) and three (bottom) intermediate qubits. The dashed box represents entanglement creation while the dotted ones swap entanglement to the next neighbors. The extra swap box is indicated in the bottom circuit

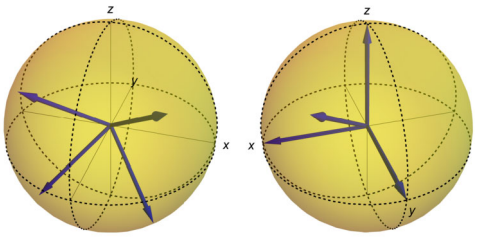

Figure 3 The Bloch vectors for the sets of measurements used in the work, left set I and right set II, in the test (a)

for B. Vectors in the set I correspond to tetrahedron vertices: $\vec{a} = (\pm 1, \pm 1, 1)/\sqrt{3}$. In the set II, $\vec{a}$ are along principal axes xyz, and the last direction is $(1, 1, 1)/\sqrt{3}$, see Fig. 3 for an illustration. In this way, we cover the maximal space of qubit states. Both sets have been tested on IBM devices belem qubits 0, 4 (with qubits 1, 3 in the middle), lagos, perth, and nairobi 0, 6 (with qubits 1, 3, 5 in the middle). The technical characteristics of the devices are given in Appendix F.

In the case (b), we create the same Bell state as in the case (a), between next neighbor qubits A and B, separated by one extra middle connector qubit, except that now $|+\rangle = |0\rangle$ and $|-\rangle = |1\rangle$, by additional Z_- and $X = |0\rangle\langle 1| + |1\rangle\langle 0|$ (also native) gates at the end. The separation makes the communication between the parties unlikely, as any reasonable crosstalk, cannot affect the next neighbors. The 5 outcomes are formally represented by fractions of projections $M_j = (1 + \vec{m}_j \cdot \vec{\sigma})/8$ for the directions $j = 1, 2, 3, 4$ in vertices of the rotated tetrahedron

$$\begin{aligned}
\vec{m}_1 &= (\sqrt{2/3}, 0, -1/\sqrt{3}),\\
\vec{m}_2 &= (0, \sqrt{2/3}, 1/\sqrt{3}),\\
\vec{m}_3 &= (-\sqrt{2/3}, 0, -1/\sqrt{3}),\\
\vec{m}_4 &= (0, -\sqrt{2/3}, 1/\sqrt{3}),
\end{aligned} \tag{10}$$

and $M_5 = 1/2$ [56]. The actual implementation requires the following measurement protocol requiring 3 qubits at each party denoted by $a_0a_1a_2$, $b_0b_1b_2$ for the party A, B, respectively, with the final results $a_j, b_j = 0, 1$ corresponding to the states $|0\rangle$, $|1\rangle$, respectively. Let us focus now on one of the parties, say A, as the other party is analogous. The initially entangled qubit of A is mapped by a $CNOT$ gate to an auxiliary one, i.e.

$$\alpha|00\rangle + \beta|10\rangle \to \alpha|00\rangle + \beta|11\rangle. \tag{11}$$

Now, we choose one of these two qubits to be a spectator qubit, a_0, while the other qubit is the working qubit a_1. We apply rotation Z_+ to the spectator qubits and subsequently S, to measure them in the x basis i.e. $(|0\rangle \pm |1\rangle)/\sqrt{2}$. In this way, the probability $p(a_0)$ is always 1/2. For $a_0 = 0, 1$, the working qubit is in the state $\alpha|0\rangle + \beta|1\rangle$ or $\alpha|0\rangle - \beta|1\rangle$, respectively. Note that the latter state differs from the first one by Z_π rotation. We finally apply Q gate to map the projections (10) of each working qubit onto the four states of the two qubits $a_1a_2 = 00, 10, 01, 11$, corresponding to outcomes 1, 2, 3, 4, see details in Appendix E and

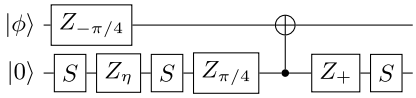

Figure 4 The Q gate mapping the working state $|\phi\rangle$ onto the 4 projections (10) for the measurements 00, 10, 01, 11. We used the angle $\eta = \arccos\sqrt{1/3}$

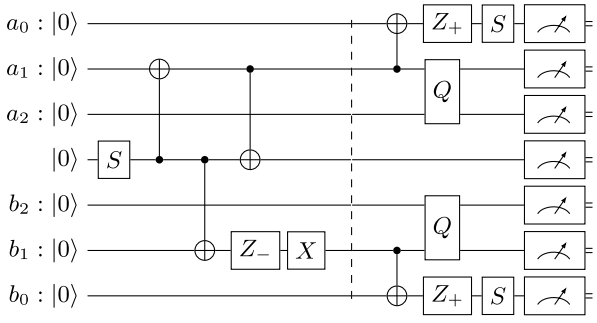

Figure 5 The test (b) using *CNOT* and Q gates (see Fig. 4) using 7 qubits, in two groups of 3 qubits, party A: $a_0a_1a_2$, party B: $b_0b_1b_2$, separated by an extra connector qubit

Fig. 4. Note that the Z rotation on Q projection simply reverses the bit a_2. The original set of 8 outcomes can be treated as 5 outcomes, depending on the spectator qubit, i.e. a chosen value a_0 defines 4 outcomes $a_0a_1a_2$ and the rest $(1 - a_0) * *$ are treated as 5 (i.e. 4 other outcomes are in a single set). Out of all 64 probabilities p_{ab}, 16 of them are zero, for $a_1 = b_1$ and $a_0 + a_2 - b_0 - b_2$ even. The remaining probabilities are each equal 1/48. The complete scheme, using *CNOT* gate is depicted in Fig. 5.

Each test consists of a certain number of jobs, where each circuit (randomly shuffled) is run a certain number of shots. Since the number of experiments is 16, each one could be repeated to saturate the limit on circuits. The total number of trials is $N = \#jobs\#shots\#repetitions$. Due to calibration changes, every several hours, the probabilities may drift, which can affect the witness being a nonlinear function of probabilities. To take it into account, we have calculated the witness in two ways [34]: W and its error is obtained from total probabilities of all jobs together, W' and its error is obtained by calculating W and the error for each job individually, and then averaging it over jobs. It turns out that these values indeed differ but do not change the verdict about Schmidt number.

For the case (a), we run 247/404 jobs on belem with 20,000 shots and 6 repetitions for sets I/II, while 20/15 jobs with 10,000 shots and 6 repetitions on lagos. An additional test has been run on perth/nairobi (set II) with 259/550 jobs, 10,000 shots and 6 repetitions. The statistics differ from the ideal ones because of the noise but agree qualitatively, see Fig. 6 and 7. The final witness agrees with the null hypothesis for $d = 2$ within the statistical error, see Table 3. No-signaling has been confirmed as a sanity check. However, in the test on perth, we found the desired value of the witness, but we also observed a moderate violation of no-signaling at the level of 3.9 standard deviations, see Appendix D. Due to 48 possible comparisons, the look-elsewhere-effect lowers the significance of this observation. Nevertheless, this difference suggests that our test may be useful in identifying malfunctions of the devices in the future.

The test (b) has been performed on nairobi, qubits 0,1,2 (A) and 6,5,4 (B) connected by 3, and brisbane, 2 groups, qubits 23,22,21 (A) and 25,26,27 (B), connected by 24, and

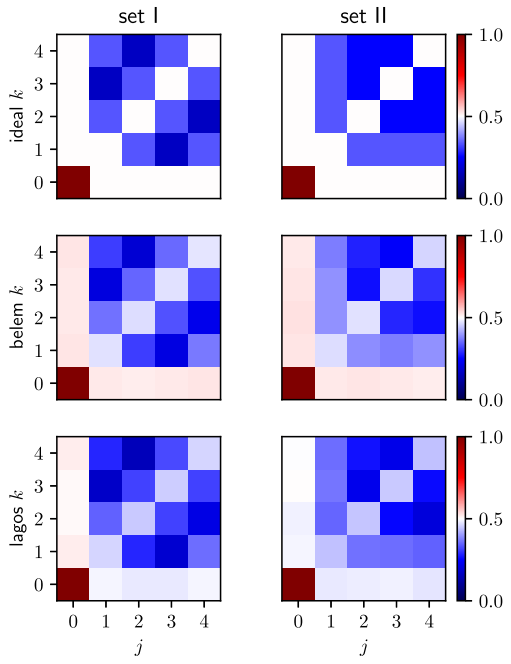

Figure 6 Results of the tests (a) with probabilities p_{kj}, for belem and lagos, compared to the ideal expectation

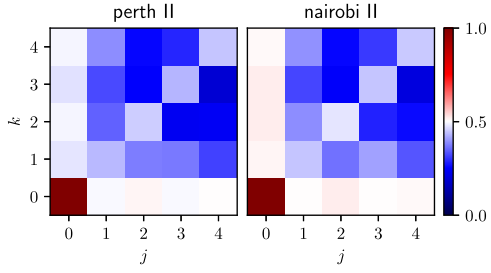

Figure 7 Results of the tests (a) with probabilities p_{kj}, for perth and nairobi

Table 3 The values of the witnesses for the test (a) with errors depending on the device and set I/II. Here W_4, W_4', errors ΔW_4, and $\Delta W_4'$ are in units 10^{-6}

device	W_4	ΔW_4	W_4'	$\Delta W_4'$
belem I	0.199	1.267	0.135	1.294
lagos I	15.69	9.08	20.52	9.75
belem II	−0.647	1.269	−3.749	1.338
lagos II	−8.233	9.782	−7.402	9.992
perth II	1.664	2.132	1.551	2.139
nairobi II	2.184	1.448	2.293	1.483

118,117,116 (A) and 120,121,122 (B) connected by 119, as depicted in Fig. 8. For nairobi, we have run 20 jobs, with 300 repetitions and 100,000 shots. For brisbane, we have run 20 jobs, 75 repetitions, and 20,000 shots. The results are presented in the Table 4. The results show the failure of the order of 6, 7, and 8 standard deviations. To explain the nonzero value of W by small corrections to probabilities of any origin, i.e. $p \to p + \delta p$, one can estimate

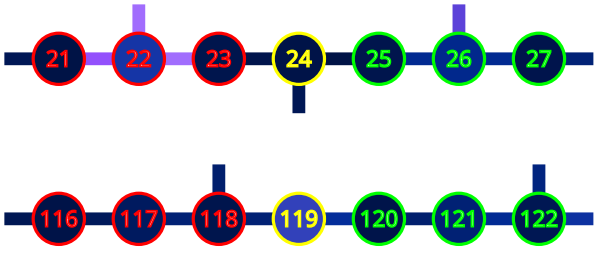

Figure 8 The tested groups of qubits on IBM Quantum brisbane. We have highlighted qubits in the test (b), parties A (red), B (green), and middle connectors (yellow). Two-qubit Echoed Cross Resonance gates, used in the test, connect the tested qubits, and the external ones

Table 4 Experimental results from the test (b) for nairobi and the two groups on brisbane, for all combinations of spectator qubit values $a_0 b_0$. Here W_4, W_4', errors ΔW_4, and $\Delta W_4'$ are in units 10^{-12}

group	$a_0 b_0$	W_4	ΔW_4	W_4'	$\Delta W_4'$
nairobi	00	46.9	7.5	56.1	8.2
0,1,2 (A)	01	−42.4	6.6	−50.3	7.2
6,5,4 (B)	10	−48.7	7.1	−54.5	7.6
	11	42.6	6.3	50.7	6.7
brisbane	00	−69.9	8.7	−69.3	9.0
23,22,21 (A)	01	68.8	9.8	67.7	10.1
25,26,27 (B)	10	64.4	8.5	65.8	8.9
	11	−62.0	9.4	−63.0	9.9
brisbane	00	−30.0	3.5	−32.4	3.8
118,117,116 (A)	01	29.5	3.4	−31.7	3.7
120,121,122 (B)	10	28.7	3.3	30.9	3.6
	11	−29.1	3.4	−31.4	3.7

$\delta W = \mathrm{Tr}\,\mathcal{A}\delta p$ for the adjugate matrix $\mathcal{A}$. The elements of the adjugate matrix are of the order $\lesssim 10^{-6}$ for nairobi and $\lesssim 10^{-7}$ for brisbane, so the result of the order $\gtrsim 10^{-11}$ would require the contribution from an extra state, beyond the assumed Hilbert space, of the order 10^{-5} or 10^{-4}. Taking into account that the entanglement is created by a single S gate with error $\lesssim 10^{-3}$ (includes leakage to higher excited states) and two $CNOT/ECR$ gates with errors $\sim 10^{-2}$ (the error includes known crosstalks), the total technical contribution would be $< 10^{-7}$ (product of error of S and two $CNOT/ECR$s to reach the parties A and B) which is much below our observation. We have checked also that the values of the witness for individual jobs are consistently nonzero and their average is close to the total values (4). The diagnostic data are summarized in Appendix F and the raw data are available publicly [57].

5 Conclusions

We have demonstrated the extreme usefulness of null tests of the Schmidt number for the bipartite states, which should help in the diagnostics of quantum devices. It is complementary to the violation of a Bell-type inequality while based on similar assumptions. Combining it with no-signaling verification and Bell-type violations in a single test can serve as a powerful quality criterion of multiqubit networks. We stress that our null hypothesis tests remain robust against most common disturbances, as long as they are local, with known mechanisms. Due to the extreme accuracy of the test, we were able to diagnose IBM Quantum devices, far beyond standard technical specifications. The results

showed consistency with the Schmidt number $d = 2$ in the case of independent measurements but the test with many outcomes failed to confirm it. The deviation is significant and exceeds possible common origins due to gate errors. The failure requires an urgent technical explanation. Otherwise, the results may be a signature of an exotic picture, involving e.g. many worlds/copies [58, 59] (N copies of the same system formally boost the dimension and Schmidt number from d to d^N). We refrain from giving an exact model, as the collected data are insufficient to draw stronger conclusions.

Appendix A: Details of the proof of the bound on W_n in the classical and quantum case

Here we present the proof of the bound on W_n over possible states and measurements. In the classical case (a), the maximization relies on basic linear algebra and the Cauchy-Binet formula for the determinant of a product of rectangular matrices. Taking two elements of ρ in a single column/row, e.g. $(1, \pm)$ and shifting $\rho_{1\pm} \to \rho_{1\pm} \pm \Delta$ results in $p_{ij} \to p_{ij} + \sum_{\pm} p_{ij}(\pm) A_{i1} B_{\pm j} \Delta$. It implies adding linearly dependent columns/rows, so by decomposing linearly columns in the new determinant to the old p and Δ entries, only terms linear in Δ are added. It means that the determinant is linear in terms of Δ and its maximum is at extremal Δ, so that one of $\rho_{1\pm}$ must be 0. Repeating this reasoning we end up with the diagonal ρ, shortening $\rho_z \equiv \rho_{zz}$. From linearity with respect to rows/columns, the maximum of $\det p$ occurs when the entries of matrices A and B are either 0 or 1.

From the Cauchy-Binet formula

$$\det p = \sum_M \det A_M \det B_M \prod_{z \in M} \rho_z \leq \sum_M \left(\det A_M^2 + \det B_M^2\right) \prod_{z \in M} \rho_z / 2, \tag{A1}$$

where M is a subset of indices to restrict columns in A and rows in B, and we use the Cauchy inequality at the end. Therefore to maximize $\det p$ we should replace A with B^T or vice versa, to obtain $p = A \rho A^T$. Then we end up with a symmetric matrix p. Let us now multiply the all rows of A except the zeroth one by 2, which makes $\det p$ multiplied by 4^n. Now subtract it from all other rows, which does not change $\det p$ but the new matrix A consists of ± 1 entries. The diagonal elements are then 1 from normalization, so $\mathrm{Tr}\, p = n + 1$. For the symmetric matrix the $\mathrm{Tr}\, p = \sum_i \lambda_i$, for eigenvalues λ_i, and $\det p = \prod_i \lambda_i$. From inequality between arithmetic and geometric means, the determinant is maximal is when all eigenvalues are equal 1, giving here 1, and finally 4^{-n} for the original determinant. The maximum is obtained when the rows of the new A are orthogonal. It suffices to have 2^n states in ρ (columns of A) and fill the first n rows in each column by its binary digits. Then our auxiliary matrix A with ± 1 entires has mutually orthogonal rows, giving the diagonal p, proportional to identity, with $\rho_i = 2^{-n}$. In fact, the number of required states is the size of the nearest Hadamard matrix (i.e. ± 1 matrix of orthogonal rows), which has a size often much smaller than 2^n.

To find the quantum maximum in both cases, let us begin with the pure state with Schmidt decomposition,

$$|\psi\rangle = \sum_k \psi_k |kk\rangle \tag{A2}$$

for real $\psi_k \geq 0$, with $\sum_k \psi_k^2 = 1$.

Now, we decompose $A = A_D + A_R + iA_I$ with real diagonal A_D, and off-diagonal A_R and A_I ($A_I = 0$ in the quantum real case), and similarly B. From Hermicity A_R is symmetric and A_I is antisymmetric. The matrix p can be expressed

$$p_{ij} = \sum_{kl} \psi_k \psi_l (A_i)_{kl} (B_j)_{kl} = \sum_k \psi_k^2 A_{Dk} B_{Dk} + \sum_{k<l} \psi_k \psi_l (A_{Rkl} B_{Rkl} - A_{Ikl} B_{Ikl}). \tag{A3}$$

Now, we can use Cauchy-Binet formula analogous to (A1), with z running over Dk, Rkl, and Ikl, just like in the classical case. We also maximize the determinant by replacing either A by $B^T = B^*$ or vice versa, noting the minus sign at I product.

The quantum maximum cannot exceed the classical one in the case (a). We can consider only projections A_i as the Cauchy-Binet formula is quadratic and convex with respect to each individual A_i, a linear combination of projections, and so the maximum requires extremal arguments. Now subtracting half of the last row and column from the other ones, and then multiplying each row and column except by 2 the last one, we replace projections A by $2A - 1$, which are observables with outcomes ± 1. The matrix is symmetric since we have a Schmidt-type entangled state and $A = B^*$ while each diagonal term is nonnegative and bounded by 1. Analogously as in the classical case, the bound on the determinant is 1, divided finally by 4^n because of doubling the values of rows and columns.

In the case (b), the maximum is classical for $d > n$. Otherwise, we can construct the diagonal matrix $\Psi = \mathrm{diag}(\sqrt{\psi_1}, \ldots, \sqrt{\psi_d})$. so that $p_{ij} = \mathrm{Tr} A_i' A_j'^T$ for $A_i' = \Psi A_i \Psi$. Let $a_i = \mathrm{Tr} A_i'$, and $A_i' = a_i \bar{A}_i$, so that $\mathrm{Tr} \bar{A}_i = 1$. Then $\sum_i a_i = \sum_i \psi_i = c$. Under this constraint, by convexity of Cauchy-Binet expansion with respect to A' we retrieve the maximal result when $\bar{A}_i$ are single-dimensional projections. Moreover, writing $\bar{p}_{ij} = \mathrm{Tr} \bar{A}_i \bar{A}_j^T$ we have $\det p = \det \bar{p} \prod_i a_i^2$. From the arithmetic and geometric mean inequality, the maximum occurs when $a_i = c/n$. The problem of maximal $\det \bar{p}$ reduces now to our previous result [55], i.e. the maximum of $\det \bar{p}$ is $(n+1)^{n+1}(d-1)^n / d^{n+1} n^n$. Finally we find the maximal $c = d^{1/2}$ when all $\psi_i = d^{-1/2}$ from the inequality between quadratic and arithmetic means, which completes the final bound.

Appendix B: Determination of classical and quantum maxima in particular cases

To find the respective maxima, we have used a hybrid approach similar to [32]. Setting the space of parameters of measurements and states, we find first the maximum numerically. Then we try to find a symmetry to represent the case using fewer parameters.

B.1 Case (a) *n* independent measurements

Case $n = 1$. $W = 0$ for $d = 1$ (classical, quantum real or complex). For $d = 2$ we reach the classical maximum for $\rho_j = 1/2$ and (omitting the last row of 1)

$$A = \begin{pmatrix} 1 & 0 \end{pmatrix}, \tag{B1}$$

giving $W = 1/4$.

Case $n = 2$. $W = 0$ for $d = 1, 2$ classical while $1/3^3$ for $d = 3$, with $\rho_j = 1/3$,

$$A = \begin{pmatrix} 1 & 0 & 0 \\ 0 & 1 & 0 \end{pmatrix}. \tag{B2}$$

The absolute maximum (from Sect. 2) is for $d = 4$, $\rho_j = 1/4$ and

$$A = \begin{pmatrix} 1 & 1 & 0 & 0 \\ 1 & 0 & 1 & 0 \end{pmatrix}. \tag{B3}$$

Case $n = 3$. $W = 0$ for $d = 1, 2, 3$ classical. The absolute maximum is for $d = 4$, $\rho_j = 1/4$, and

$$A = \begin{pmatrix} 1 & 1 & 0 & 0 \\ 1 & 0 & 1 & 0 \\ 1 & 0 & 0 & 1 \end{pmatrix}. \tag{B4}$$

Case $n = 4$. $W = 0$ for $d \leq 4$ classical. For $d = 5$, $\rho_j = 1/5$, and

$$A = \begin{pmatrix} 1 & 1 & 0 & 0 & 0 \\ 1 & 0 & 1 & 0 & 0 \\ 1 & 0 & 0 & 1 & 0 \\ 1 & 0 & 0 & 0 & 1 \end{pmatrix}, \tag{B5}$$

we get $W = 9/5^5$.

For $d = 6$,

$$A = \begin{pmatrix} 1 & 1 & 0 & 0 & 0 & 1 \\ 1 & 0 & 1 & 0 & 0 & 1 \\ 0 & 0 & 0 & 0 & 1 & 1 \\ 0 & 1 & 1 & 0 & 0 & 1 \end{pmatrix}, \tag{B6}$$

and $\rho = \mathrm{diag}(x, x, x, z, y, y)$ with $z = 1 - 3x - 2y$, gives $W = 0.002954143422708182$, $x = 0.19585843826556898$, $y = 0.18219100818175962$.

For $d = 7$,

$$A = \begin{pmatrix} 0 & 0 & 0 & 0 & 0 & 1 & 1 \\ 0 & 0 & 0 & 1 & 1 & 1 & 0 \\ 0 & 0 & 1 & 1 & 0 & 0 & 1 \\ 0 & 1 & 0 & 0 & 1 & 0 & 1 \end{pmatrix}, \tag{B7}$$

with $\rho = \mathrm{diag}(w, x, x, y, y, z, z)$ and $w = 1 - 2x - 2y - 2z$. The numerical maximum is $W = 0.0030764392399879$ for $x = 0.06135153414853146$, $y = 0.1710023907787869$, $z = 0.19069830365543322$.

The absolute maximum occurs for $d = 8$ and

$$A = \begin{pmatrix} 0 & 1 & 0 & 1 & 1 & 0 & 0 & 1 \\ 0 & 0 & 0 & 1 & 0 & 1 & 1 & 1 \\ 0 & 1 & 1 & 0 & 0 & 0 & 1 & 1 \\ 0 & 0 & 1 & 0 & 1 & 1 & 0 & 1 \end{pmatrix}, \tag{B8}$$

with $\rho_j = 1/8$.

Case $n = 5$. For $d = 6$ and

$$A = \begin{pmatrix} 1 & 0 & 1 & 0 & 0 & 0 \\ 0 & 1 & 1 & 1 & 0 & 1 \\ 1 & 1 & 0 & 0 & 0 & 1 \\ 1 & 0 & 0 & 1 & 0 & 1 \\ 0 & 0 & 1 & 0 & 1 & 1 \end{pmatrix}, \tag{B9}$$

and $\rho_j = 1/6$ we get $W = 5^2/6^6$.

For $d = 7$ we get $W = 12^{-3}$ for

$$A = \begin{pmatrix} 0 & 1 & 0 & 0 & 0 & 1 & 1 \\ 0 & 1 & 0 & 1 & 1 & 0 & 0 \\ 0 & 0 & 1 & 1 & 0 & 1 & 0 \\ 0 & 0 & 1 & 0 & 1 & 0 & 1 \\ 0 & 1 & 1 & 0 & 0 & 0 & 0 \end{pmatrix}, \tag{B10}$$

and $\rho = \mathrm{diag}(1/6, 1/6, 1/6, 1/8, 1/8, 1/8, 1/8)$.

The absolute maximum occurs for $d = 8$, $\rho_j = 1/8$ and

$$A = \begin{pmatrix} 0 & 0 & 0 & 0 & 1 & 1 & 1 & 1 \\ 0 & 0 & 1 & 1 & 0 & 1 & 1 & 0 \\ 0 & 1 & 1 & 0 & 1 & 0 & 1 & 0 \\ 1 & 0 & 1 & 0 & 0 & 0 & 1 & 1 \\ 1 & 0 & 1 & 0 & 1 & 1 & 0 & 0 \end{pmatrix}. \tag{B11}$$

Quantum case $n = 2$, $d = 2$. Bell state $|\psi\rangle = (|12\rangle - |21\rangle)/\sqrt{2}$ with $A_j = B_j = |v_j\rangle\langle v_j|$ and $|v_1\rangle = |1\rangle$, $v_2\rangle = (|1\rangle + |2\rangle)/\sqrt{2}$ gives the absolute maximum.

Quantum case $n = 3$, $d = 2$, zero in the real case. Complex: the same Bell state but adding $|v_3\rangle = (|1\rangle + i|2\rangle)/\sqrt{2}$ gives the absolute maximum up to a sign, depending on ordering.

Quantum case $n = d = 3$ (real). The state reads

$$|\psi\rangle = p|11\rangle + q\big(|22\rangle + |33\rangle\big), \tag{B12}$$

with $A_j = B_j = |v_j\rangle\langle v_j|$, and

$$|v_j\rangle = s|1\rangle + w\big(\cos(2j\pi/3)\big|2\rangle + \sin(2j\pi/3)\big|3\rangle\big), \tag{B13}$$

constrained by $p^2 + 2q^2 = s^2 + w^2 = 1$ which gives the maximal $W = 0.013208219549514474$ for $q = 0.5080857929626221$, $s = 0.7236153449503123$.

Quantum case $n = 4$, $d = 3$ real. We take

$$|\psi\rangle = \big(2|11\rangle + \sqrt{3}\big(|22\rangle + |33\rangle\big)\big)/\sqrt{10}, \tag{B14}$$

and $A_j = B_j = |v_j\rangle\langle v_j|$, with

$$v_{1,2} = s_1|1\rangle \pm w_1|2\rangle, v_{3,4} = s_2|1\rangle \pm w_2|3\rangle, \tag{B15}$$

and $s_{1,2}^2 = (9 \pm \sqrt{17})/16$, $w_{1,2}^2 = (7 \pm \sqrt{17})/16$, giving $W = 27/12{,}500$. In the complex case

$$|\psi\rangle = p|11\rangle + q|22\rangle + r|33\rangle, \tag{B16}$$

and

$$|v_j\rangle = a\big|1\rangle + x\omega^j\big|2\rangle + y\omega^j|3\rangle, \tag{B17}$$

for $j = 1, 2, 3$ and $\omega = e^{2\pi i/3} = (i\sqrt{3} - 1)/2$ while $|v_4\rangle = b|2\rangle + c|3\rangle$. Maximizing with constraints $p^2 + q^2 + r^2 = a^2 + x^2 + y^2 = b^2 + c^2 = 1$ we get $W = 0.003065301182016068$ for $x = -0.20660676061609246$, $y = 0.8141407994847997$, $b = 0.5366502440643837$, $c = 0.8438048656782298$, $q = 0.45755959305674204$, $r = 0.6898510489488422$.

Quantum case $n = 5$, $d = 3$ real. Then $|\psi\rangle = (|11\rangle + |22\rangle + |33\rangle)/\sqrt{3}$ and

$$|v_j\rangle = a\big(\cos(2\pi j/5)\big|1\rangle + \sin(2\pi j/5)\big|2\rangle\big) + b|3\rangle$$

with $a^2 + b^2 = 1$. We get the maximum

$$W = (2437 + 340\sqrt{10})/(2 \cdot 3^{14}) \simeq 0.0003671542094938571$$

for $a^2 = (10 + \sqrt{10})/15$.

Complex case. We take $|\psi\rangle = p|11\rangle + q|22\rangle + r|33\rangle$ and $|v_j\rangle = x\zeta^j|1\rangle + y|2\rangle + z\zeta^{-j}|3\rangle$ with $\zeta = e^{2\pi i/5}$. Maximizing with constraints $p^2 + q^2 + r^2 = x^2 + y^2 + z^2 = 1$ we get $W = 0.000674047929103352$, $x = 0.7998181925131095$, $z = -0.4434461617437569$, $p = 0.6838826680323404$, $r = 0.5298910387696789$.

Quantum $n = 6$, $d = 3$ complex. The state $|\psi\rangle = \sqrt{2/7}(|11\rangle + |22\rangle) + \sqrt{3/7}|33\rangle$ and $|v_j\rangle = (|1\rangle + \omega^j|3\rangle)/\sqrt{2}$, $|v_{j+3}\rangle = (|2\rangle + \sqrt{2}\omega^j|3\rangle)/\sqrt{3}$ returns $W = 4 \cdot 27/7^7$.

Quantum $n = 7$, $d = 3$ complex. We take $|\psi\rangle = \sqrt{5}(|11\rangle + |22\rangle)/4 + \sqrt{6}|33\rangle/4+$ and $|v_{j+3m}\rangle = x_m|1\rangle + y_m|2\rangle + z_m\omega^j|3\rangle$ for $j = 1, 2, 3$, $m = 0, 1$ and $|v_7\rangle = |1\rangle$ Then the numerical maximum with constraints $x_m^2 + y_m^2 + z_m^2 = 1$ is $W = 0.0000215113826$.

Quantum $n = 8$, $d = 3$ complex. $|\psi\rangle = (|11\rangle + |22\rangle + |33\rangle)/\sqrt{3}$ with $|v_j\rangle = \sqrt{10}|1\rangle/6 \pm i|2\rangle/\sqrt{6} + \sqrt{5}\omega^j|3\rangle/3$ for $j = 1 \ldots 6$ while $|v_{7,8}\rangle = \sqrt{5/6}|1\rangle \pm |2\rangle/\sqrt{6}$ which gives $W = 5^{10}/3^{26}$.

B.2 Case (b) single measurement with $n + 1$ outcomes

It is convenient to consider positive Hermitian matrices $A_i' = \sqrt{Z}\Psi A_i \Psi$, which are not normalized, giving $p_{ij}' = \mathrm{Tr}\, A_i' A_j'$ and normalize probability by $p = p'/Z$ with $Z = \mathrm{Tr}\, A^2$ for $A = \sum_i A_i'$. The state is then reconstructed as $\Psi^2 = A/\sqrt{Z}$ in its diagonal basis. Similarly

as in [55] we focus on matrices of rank $\leq d/2$. Otherwise, the overlapping projection is free to shift between the matrices with the linear change of the determinant. In the case $n = 4$, $d = 3$ we could reduce $i < 5$ to rank 1. The last matrix $i = 5$ could have rank 2, but our numerical analysis showed that the optimal case is also of rank 1. The result in the real case $A'_j = |v_j\rangle\langle v_j|$ with

$$\begin{aligned}
&|v_{1,2}\rangle = x|1\rangle \pm y|2\rangle,\\
&|v_{3,4}\rangle = a|1\rangle \pm b|3\rangle,\\
&|v_5\rangle = z|2\rangle,
\end{aligned} \tag{B18}$$

with $a^4 = 1/160$, $b^4 = 1/120$, $y = 3b$, $x = 4a$, $z = 12b$ giving $W = 1.6875 \cdot 10^{-5}$ (exact).

In the complex case, $A'_j = |v_j\rangle\langle v_j|/Z$ with

$$\begin{aligned}
&|v_j\rangle = a|j\rangle, j = 1, 2,\\
&|v_j\rangle = q\omega^j\big|1\rangle + q\omega^{2j}\big|2\rangle + r|3\rangle, j = 3, 4, 5,
\end{aligned} \tag{B19}$$

with $\omega = e^{2\pi i/3} = (\sqrt{3}i - 1)/2$, $a^2 = 3q^2(q^2 + 2r^2)/(q^2 + r^2)$ and $Z = 9(2q^4(2q^2 + 3r^2)^2 + r^4(q^2 + r^2)^2)/(q^2 + r^2)$. As the determinant is a homogenous function of q and r, setting $q = 1$ and $r^2 = x$ we end up with

$$W = \frac{x^2(1 + x)^6(1 + 2x)^6)}{27(x^2(1 + x)^2 + 2(2 + 3x)^2)^5}, \tag{B20}$$

reaching its maximum $1.874577768244 \cdot 10^{-5}$ for x being the largest root of

$$x^4 + 2x^3 - 11x^2 - 11x - 2 = 0, \tag{B21}$$

i.e. $x = 2.98813453198126056781$.

Appendix C: Counterexample to prepare and measure scenario

In [33], one considers $W_7 = \det p$ for the matrix p with entries $p_{ij} = p(i|2j) - p(i|2j + 1)$ for $p(k|i)$ for $i = 0 \ldots 6$, and $j = 0 \ldots 13$ being the probability of 1 the ith dichotomic measurement on the state k [30]. It is claimed that $W_7 = 0$ in the case of a bipartite state consisting of two independent qubits. We shall present a counterexample to this claim.

Let us take a state in the Pauli basis $|\vec{a}\rangle = ((1 + a_z)|0\rangle + (a_x + ia_y)|1\rangle)/2$ so that the probability of the $p(a|c) = |\langle\vec{c}|\vec{a}\rangle|^2 = (1 + \vec{a} \cdot \vec{c})/2$. Generalizing it to two independent qubits, we have $p(a, b|c, d) = (1 + \vec{a} \cdot \vec{c})(1 + \vec{b} \cdot \vec{d})/4$. We take the states and measurements as follows

$$\begin{aligned}
&\vec{c}_{0,1,2} = (1, 0, 0),\ \vec{c}_{3,4,5} = (0, 1, 0),\ \vec{c}_6 = (0, 0, 1),\\
&\vec{d}_{0,3,6} = (1, 0, 0),\ \vec{d}_{1,4} = (0, 1, 0), \vec{d}_{2,5} = (0, 0, 1),\\
&\vec{a}_{0,2,4} = (1, 0, 0) = -\vec{a}_{1,3,5} = (-1, 0, 0),\\
&\vec{a}_{6,8,10} = (0, 1, 0) = -\vec{a}_{7,9,11},
\end{aligned}$$

$$\vec{a}_{8,10,12} = (0,0,1) = -\vec{a}_{9,11,13},$$
$$\vec{b}_{0,6,12} = (1,0,0),\ \vec{b}_{2,8} = (0,1,0),\ \vec{b}_{4,10} = (0,0,1), \tag{C1}$$

with $\vec{b}_{1,3,5} = -\vec{b}_{0,2,4}$ and $\vec{b}_{7,9,11,13} = \vec{b}_{6,8,10,12}$. Then

$$W(i,j) = p(i,2j) - p(i,2j+1) = \begin{cases} (\vec{c}_i \cdot \vec{a}_{2j} + \vec{d}_i \cdot \vec{b}_{2j})/2 & \text{for } j < 3, \\ \vec{c}_i \cdot \vec{a}_{2j}(1 + \vec{d}_i \cdot \vec{b}_{2j})/2 & \text{for } j \geq 3. \end{cases} \tag{C2}$$

The matrix p reads

$$\begin{pmatrix} 1 & 1/2 & 1/2 & 0 & 0 & 0 & 0 \\ 1/2 & 1 & 1/2 & 0 & 0 & 0 & 0 \\ 1/2 & 1/2 & 1 & 0 & 0 & 0 & 0 \\ 1/2 & 0 & 0 & 1 & 1/2 & 1/2 & 0 \\ 0 & 1/2 & 0 & 1/2 & 1 & 1/2 & 0 \\ 0 & 0 & 1/2 & 1/2 & 1/2 & 1 & 0 \\ 1/2 & 0 & 0 & 1/2 & 0 & 0 & 1/2 \end{pmatrix}, \tag{C3}$$

whose determinant is 1/8. It means that $W_7 \neq 0$ contrary to the general claim of [33]. We suspect that equality $W_7 = 0$ requires additional assumptions on preparations and measurements.

Appendix D: No-signaling

The crucial assumption of the test (a) is locality. One can only verify a consequence of locality, namely no-signaling. It means that the probability p_{i0} and p_{0j} can be found in any (i,j) pair of measurements as $p_{i0,j}$ or $p_{0j,i}$, but does not depend on the other party, i.e.

$$p_{i0,j} = p_{i0},\ p_{0j,i} = p_{0j}. \tag{D1}$$

In our demonstration, we could determine each $p_{i0,j}$ and $p_{0j,i}$, i.e. $2 \times 4 \times 4$ numbers. The results are presented in Figs. 9, 10, 11, 12, 13, 14. In the case of belem, lagos, and nairobi, no-signaling is satisfied within the statistical error. However, for perth, $p_{20,1}$ differs from $p_{20,2}$ by 3.9 standard deviations, corresponding to p-value 10^{-4}.

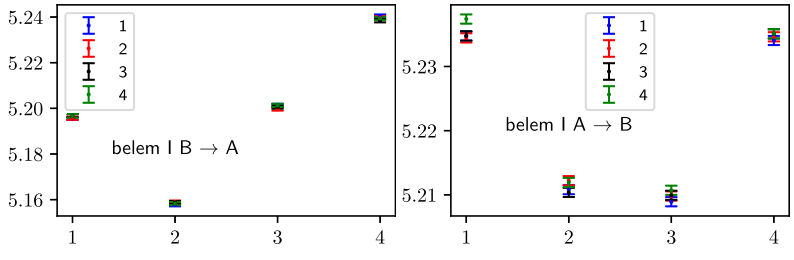

Figure 9 No-signaling test for belem I, for (top) p_{i0} (i on the horizontal axis) depending on j (inset), and (bottom) p_{0j} depending on i

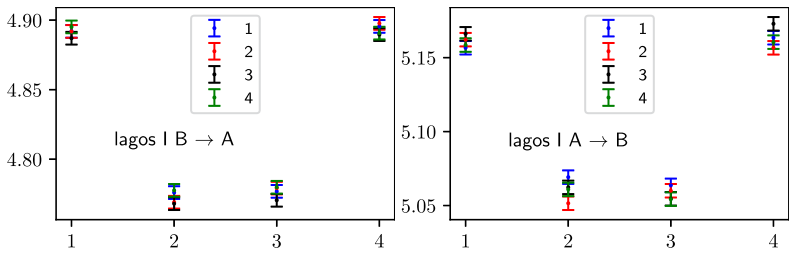

Figure 10 No-signaling test for lagos I, notation as in Fig. 9

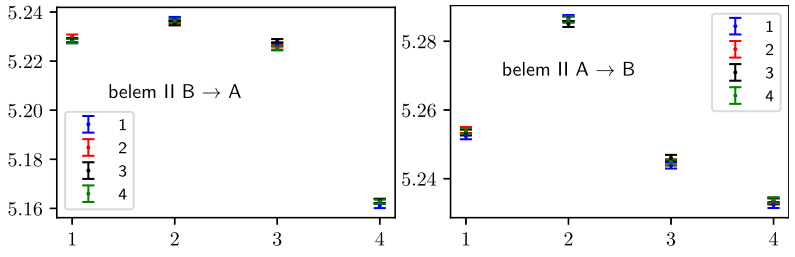

Figure 11 No-signaling test for belem II, notation as in Fig. 9

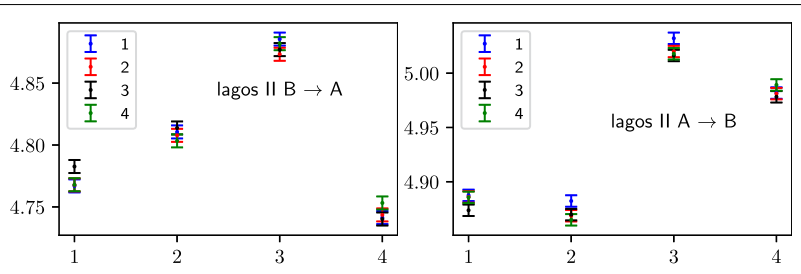

Figure 12 No-signaling test for lagos II, notation as in Fig. 9

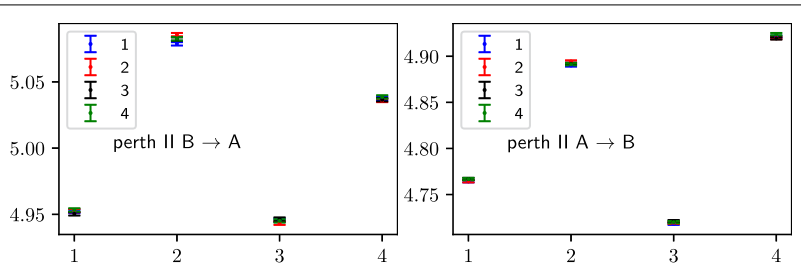

Figure 13 No-signaling test for perth II, notation as in Fig. 9

The actual significance is lower because of 48 possible comparisons, due to the look-elsewhere effect. Nevertheless, we suggest caution and repeating this test with different resources.

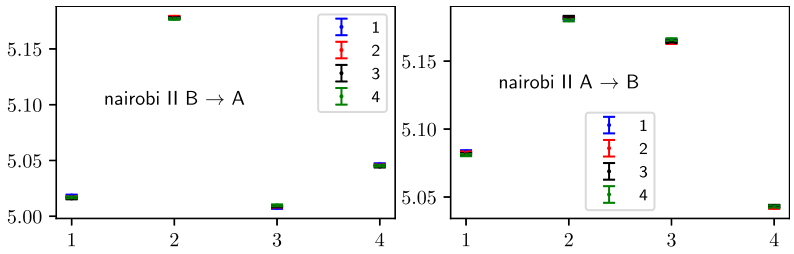

Figure 14 No-signaling test for nairobi II, notation as in Fig. 9

Figure 15 The notation of the ECR gate in the convention $ECR_{\downarrow}|ab\rangle$

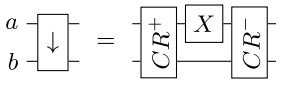

Appendix E: Relation between *CNOT* and *ECR* gates

The IBM Quantum devices (brisbane) use a native two-qubit gate Echoed Cross Resonance (*ECR*) instead of *CNOT*. However, one can transpile the latter by the former, adding single qubits gates. We shall use Pauli matrices in the basis $|0\rangle$, $|1\rangle$,

$$X = \begin{pmatrix} 0 & 1 \\ 1 & 0 \end{pmatrix}, \; Y = \begin{pmatrix} 0 & -i \\ i & 0 \end{pmatrix}, \; Z = \begin{pmatrix} 1 & 0 \\ 0 & -1 \end{pmatrix}, \; I = \begin{pmatrix} 1 & 0 \\ 0 & 1 \end{pmatrix}. \tag{E1}$$

We also denote two-qubits gates by $\downarrow$ and $\uparrow$, which mean the direction of the gate (it is not symmetric), i.e. $\langle a'b'|G_{\uparrow}|ab\rangle = \langle b'a'|G_{\downarrow}|ba\rangle$.

The *ECR* gate acts on the states $|ab\rangle$ as (Fig. 15)

$$ECR_{\downarrow} = (XI - YX)/\sqrt{2} = CR^{-}(XI)CR^{+} = \begin{pmatrix} 0 & X_{-} \\ X_{+} & 0 \end{pmatrix} = \begin{pmatrix} 0 & 0 & 1 & i \\ 0 & 0 & i & 1 \\ 1 & -i & 0 & 0 \\ -i & 1 & 0 & 0 \end{pmatrix} /\sqrt{2}, \tag{E2}$$

in the basis $|00\rangle$, $|01\rangle$, $|10\rangle$, $|11\rangle$ where the native gate is

$$S = \sqrt{-iX} = X_{+} = X_{\pi/2} = (I - iX)/\sqrt{2} = \begin{pmatrix} 1 & -i \\ -i & 1 \end{pmatrix} /\sqrt{2}, \tag{E3}$$

and $X_{-} = X_{-\pi/2} = ZX_{+}Z$, with

$$CR^{\pm} = (ZX)_{\pm\pi/4}, \tag{E4}$$

using the convention $V_{\theta} = \exp(-i\theta V/2) = \cos(\theta/2) - iV\sin(\theta/2)$ if $V^2 = I$ or II. The gate is its inverse, i.e. $ECR_{\downarrow}ECR_{\downarrow} = II$.

Note that $Z_{\theta} = \exp(-i\theta Z/2) = \mathrm{diag}(e^{-i\theta/2}, e^{i\theta/2})$ is a virtual gate adding essentially the phase shift to next gates. *ECR* gates can be reversed, i.e., for $a \leftrightarrow b$, (Fig. 16)

$$ECR_{\uparrow} = (IX - XY)/\sqrt{2} = (HH)ECR_{\downarrow}(Y_{+}Y_{-}), \tag{E5}$$

Figure 16 The $ECR_{\uparrow}$ gate expressed by $ECR_{\downarrow}$

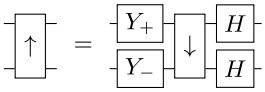

Figure 17 The $CNOT_{\downarrow}$ gate expressed by $ECR_{\downarrow}$

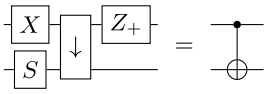

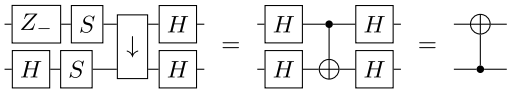

Figure 18 The $CNOT_{\uparrow}$ gate expressed by $ECR_{\downarrow}$

denoting $V_{\pm} = V_{\pm\pi/2}$, and Hadamard gate,

$$H = (Z + X)/\sqrt{2} = Z_{+}SZ_{+} = \begin{pmatrix} 1 & 1 \\ 1 & -1 \end{pmatrix}/\sqrt{2}, \tag{E6}$$

and $Z_{\pm}SZ_{\mp} = Y_{\pm}$, with $Y_{+} = HZ$ and $Y_{-} = ZH$.

The *CNOT* gate can be expressed by *ECR* (Fig. 17)

$$CNOT_{\downarrow} = (II + ZI + IX - ZX)/2 = \begin{pmatrix} I & 0 \\ 0 & X \end{pmatrix} = \begin{pmatrix} 1 & 0 & 0 & 0 \\ 0 & 1 & 0 & 0 \\ 0 & 0 & 0 & 1 \\ 0 & 0 & 1 & 0 \end{pmatrix} = (Z_{+}I)ECR_{\downarrow}(XS), \tag{E7}$$

while its reverse reads (Fig. 18)

$$\begin{aligned} CNOT_{\uparrow} &= (II + IZ + XI - XZ)/2 = \begin{pmatrix} 1 & 0 & 0 & 0 \\ 0 & 0 & 0 & 1 \\ 0 & 0 & 1 & 0 \\ 0 & 1 & 0 & 0 \end{pmatrix} \\ &= (HH)CNOT_{\downarrow}(HH) = (HH)ECR_{\downarrow}(SS)(Z\_H). \end{aligned} \tag{E8}$$

Appendix F: Experimental data

The technical characteristics of the relevant qubits and two-qubit connecting gates are shown in Table 5 and 6. the actual maps of probabilities in the case of test (b) are shown in Fig. 19. The results of the witness in the case (b) for individual jobs are presented in Fig. 20.

Table 5 The characteristics of the single qubits used in the demonstration, frequency between 0 and 1 level, anharmonicity (frequency between 1 and 2 levels above 0-1 transition), error of the gate $S = \sqrt{-iX}$ used in the tests. The duration of the single gate pulse is always 35 ns, except brisbane with 60 ns

device/qubit	freq. (GHz)	anh. (GHz)	S error [10^{-4}]
belem 0	5.09	–0.34	1.8
belem 1	5.25	–0.32	6
belem 3	5.17	–0.33	2.3
belem 4	5.26	–0.33	2.3
lagos 0	5.24	–0.34	3
lagos 1	5.10	–0.34	1.8
lagos 3	4.99	–0.345	2.3
lagos 5	5.18	–0.34	1.9
lagos 6	5.06	–0.34	1.9
perth 0	5.16	–0.34	3
perth 1	5.03	–0.34	2.5
perth 3	5.13	–0.345	2.2
perth 5	4.98	–0.34	2.8
perth 6	5.16	–0.34	2.9
nairobi 0	5.26	–0.34	2.8
nairobi 1	5.17	–0.34	3.4
nairobi 2	5.27	–0.34	3.8
nairobi 3	5.03	–0.34	4.2
nairobi 4	5.18	–0.34	2.5
nairobi 5	5.29	–0.34	3.9
nairobi 6	5.13	–0.34	1.6
brisbane 21	4.97	0.31	2.1
brisbane 22	5.04	0.31	3.9
brisbane 23	4.84	0.31	2.1
brisbane 24	5.01	0.31	2.7
brisbane 25	4.95	0.31	3.5
brisbane 26	4.85	0.31	2.7
brisbane 27	4.75	0.31	1.4
brisbane 116	4.91	0.31	1.3
brisbane 117	4.83	0.31	4.0
brisbane 118	4.73	0.31	1.4
brisbane 119	4.80	0.31	2.7
brisbane 120	4.84	0.31	3.1
brisbane 121	4.97	0.31	3.6
brisbane 122	4.94	0.31	3.0

Table 6 The errors of the two-qubit gates used in the demonstration, *CNOT* for nairobi and *ECR* for brisbane

device	connection	*CNOT*/*ECR* error [10^{-3}]
nairobi	0-1	9.2
nairobi	1-3	6.5
nairobi	1-2	8.5
nairobi	3-5	16.1
nairobi	4-5	4.8
nairobi	5-6	6.1
brisbane	21-22	5.2
brisbane	22-23	7.1
brisbane	24-23	6.6
brisbane	25-24	7.1
brisbane	26-25	10.1
brisbane	27-26	6.1
brisbane	116-117	6.1
brisbane	117-118	5.7
brisbane	118-119	11.5
brisbane	120-119	20.5
brisbane	121-120	7.3
brisbane	122-121	10.4

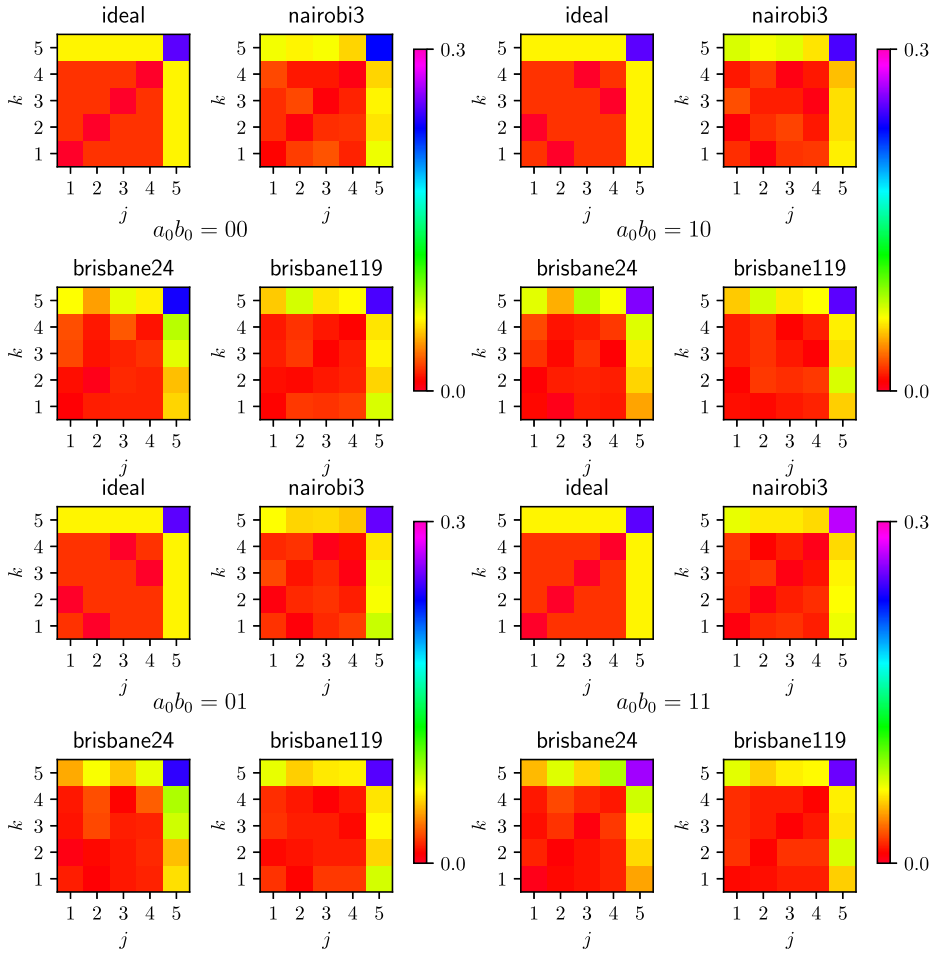

Figure 19 The probabilities for the test (b) for each combination of spectator qubits a_0b_0, see main text, with the middle qubit 3 (nairobi), 24 and 119 (brisbane), compared to the ideal theoretical expectation

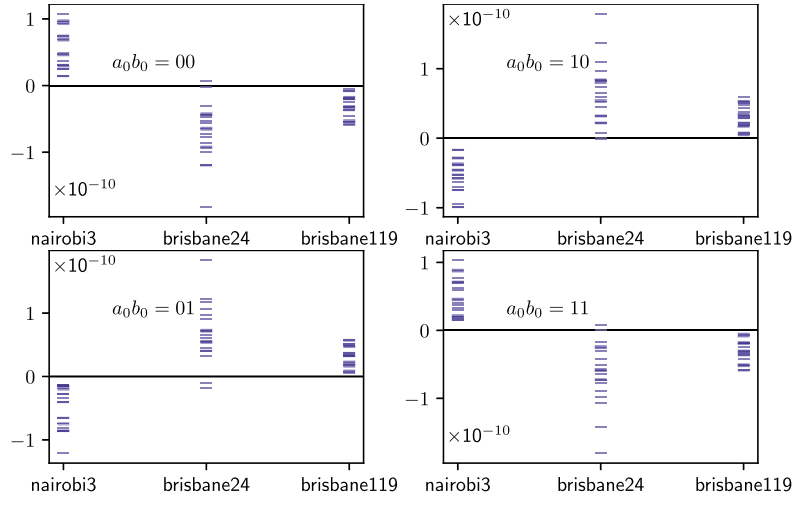

Figure 20 The results of the witness calculated for individual jobs in the test (b) for each combination of chosen spectator qubits values a_0b_0, see main text, with the middle qubit 3 (nairobi), 24, and 119 (brisbane)

Abbreviations
ECR, echoed cross-resonance..

Acknowledgements
The results have been created using IBM Quantum. The views expressed are those of the authors and do not reflect the official policy or position of IBM Quantum team. The project is co-financed by the funds of the Polish Ministry of Education and Science under the program entitled International Co-Financed Projects. TR gratefully acknowledges the funding support by the program „Excellence initiative research university" for the AGH University in Krakow as well as the ARTIQ project: UMO-2021/01/2/ST6/00004 and ARTIQ/0004/2021.

Author contributions
J.B. and A.B. developed the idea. T.B. and T.R. wrote computer scripts. J.T and A.B. wrote the manuscript. All authors reviewed the manuscript.

Funding
TR gratefully acknowledges the funding support by the program „Excellence initiative research university" for the AGH University in Krakow as well as the ARTIQ project: UMO-2021/01/2/ST6/00004 and ARTIQ/0004/2021.

Data Availability
Data is provided in European Organization For Nuclear Research and Open AIRE, Zenodo, CERN, 2021, https://doi.org/10.5281/zenodo.8358855.

Declarations

Ethics approval and consent to participate
Not applicable.

Consent for publication
Not applicable.

Competing interests
The authors declare no competing interests.

Author details
[1]Departament de Fisica and Institut d'Aplicacions Computacionals de Codi Comunitari (IAC3), Campus UIB, E-07122 Palma de Mallorca, Balearic Islands, Spain. [2]CRISP – Centre de Recerca Independent de sa Pobla, 07420, sa Pobla, Balearic Islands, Spain. [3]Faculty of Physics, University of Warsaw, ul. Pasteura 5, PL02-093 Warsaw, Poland. [4]Systems Research Institute, Polish Academy of Sciences, 6 Newelska Street, PL01-447 Warsaw, Poland. [5]Nicolaus Copernicus Astronomical Center, Polish Academy of Sciences, 18 Bartycka Street, PL00-716 Warsaw, Poland. [6]Center of Excellence in Artificial Intelligence, AGH University, 30 Mickiewicza Lane, PL30-059 Cracow, Poland.

Received: 25 July 2024 Accepted: 13 September 2024 Published online: 27 September 2024

References
1. Einstein A, Podolsky B, Rosen N. Can quantum-mechanical description of physical reality be considered complete? Phys Rev. 1935;47:777.
2. Bell JS. On the Einstein Podolsky Rosen paradox. Physics. 1964;1:195.
3. Clauser JF, Horne MA, Shimony A, Holt RA. Proposed experiment to test local hidden-variable theories. Phys Rev Lett. 1969;23:880.
4. Clauser JF, Horne MA. Experimental consequences of objective local theories. Phys Rev D. 1974;10:526.
5. Eberhard PH. Background level and counter efficiencies required for a loophole-free Einstein-Podolsky-Rosen experiment. Phys Rev A. 1993;47:R747.
6. Wiseman HM, Jones SJ, Doherty AC. Steering, entanglement, nonlocality, and the Einstein-Podolsky-Rosen paradox. Phys Rev Lett. 2007;98:140402.
7. Uola R, Costa ACS, Nguyen HC, Gühne O. Quantum steering. Rev Mod Phys. 2020;92:015001.
8. Bennett CH, Brassard G, Crepeau C, Jozsa R, Peres A, Wootters WK. Teleporting an unknown quantum state via dual classical and Einstein-Podolsky-Rosen channels. Phys Rev Lett. 1993;70:1895.
9. Pirandola S, Eisert J, Weedbrook C, Furusawa A, Braunstein SL. Advances in quantum teleportation. Nat Photonics. 2015;9:641.
10. Suzuki Y, Endo S, Fujii K, Tokunaga Y. Quantum error mitigation as a universal error reduction technique: applications from the NISQ to the fault-tolerant quantum computing eras. Phys Rev X Quantum. 2022;3:010345.
11. Takagi R, Endo S, Minagawa S, Gu M. Fundamental limits of quantum error mitigation. npj Quantum Inf. 2022;8:114.
12. Cai Z, et al. Quantum Error Mitigation. Rev Mod Phys. 2023;95:045005.
13. Gallego R, Brunner N, Hadley C, Acin A. Device-independent tests of classical and quantum dimensions. Phys Rev Lett. 2010;105:230501.
14. Brunner N, Navascues M, Vertesi T. Dimension witnesses and quantum state discrimination. Phys Rev Lett. 2013;110:150501.
15. Hendrych M, Gallego R, Micuda M, Brunner N, Acin A, Torres JP. Experimental estimation of the dimension of classical and quantum systems. Nat Phys. 2012;8:588.
16. Ahrens J, Badziag P, Cabello A, Bourennane M. Experimental device-independent tests of classical and quantum dimensionality. Nat Phys. 2012;8:592.

17. Ahrens J, Badziag P, Pawlowski M, Zukowski M, Bourennane M. Experimental tests of classical and quantum dimensions. Phys Rev Lett. 2014;112:140401.
18. Strikis A, Datta A, Knee GC. Quantum leakage detection using a model-independent dimension witness. Phys Rev A. 2019;99:032328.
19. Brunner N, Pironio S, Acin A, Gisin N, Méthot AA, Scarani V. Testing the dimension of Hilbert spaces. Phys Rev Lett. 2008;100:210503.
20. Vertesi T, Pal KF. Bounding the dimension of bipartite quantum systems. Phys Rev A. 2009;79:042106.
21. Pal KF, Vertesi T. Efficiency of higher-dimensional Hilbert spaces for the violation of Bell inequalities. Phys Rev A. 2008;77:042105.
22. Cong W, Cai Y, Bancal J-D, Scarani V. Witnessing irreducible dimension. Phys Rev Lett. 2017;119:080401.
23. Pan AK, Mahato SS. Device-independent certification of the Hilbert-space dimension using a family of Bell expressions. Phys Rev A. 2020;102:052221.
24. Collins D, Gisin N, Linden N, Massar S, Popescu S. Bell inequalities for arbitrarily high-dimensional systems. Phys Rev Lett. 2002;88:040404.
25. Sorkin R. Quantum mechanics as quantum measure theory. Mod Phys Lett A. 1994;9:3119.
26. Sinha U, Couteau C, Jennewein T, Laflamme R, Weihs G. Ruling out multi-order interference in quantum mechanics. Science. 2010;329:418.
27. Park DK, Moussa O, Laflamme R. Three path interference using nuclear magnetic resonance: a test of the consistency of Born's rule. New J Phys. 2012;14:113025.
28. Pleinert M-O, von Zanthier J, Lutz E. Many-particle interference to test Born's rule. Phys Rev Res. 2020;2:012051(R).
29. Born M. Quantenmechanik der Stossvorgänge. Z Phys. 1926;37:863.
30. Bowles J, Quintino MT, Brunner N. Certifying the dimension of classical and quantum systems in a prepare-and-measure scenario with independent devices. Phys Rev Lett. 2014;112:140407.
31. Chen X, Redeker K, Garthoff R, Rosenfeld W, Wrachtrup J, Gerhardt I. Certified randomness from remote state preparation dimension witness. Phys Rev A. 2021;103:042211.
32. Batle J, Bednorz A. Optimal classical and quantum real and complex dimension witness. Phys Rev A. 2022;105:042433.
33. Sun Y-N, et al. Experimental certification of quantum dimensions and irreducible high-dimensional quantum systems with independent devices. Optica. 2020;7:1073.
34. Białecki T, Rybotycki T, Batle J, Tworzydło J, Bednorz A. Precise certification of a qubit space. EPJ Quantum Technol. 2024;11:21.
35. Christensen BG, Liang Y-C, Brunner N, Gisin N, Kwiat PG. Exploring the limits of quantum nonlocality with entangled photons. Phys Rev X. 2015;5:041052.
36. Terhal BM, Horodecki P. Schmidt number for density matrices. Phys Rev A. 2000;61:040301(R).
37. Sanpera A, Bruss D, Lewenstein M. Schmidt-number witnesses and bound entanglement. Phys Rev A. 2001;63:050301(R).
38. Liu S, He Q, Huber M, Gühne O, Vitagliano G. Characterizing entanglement dimensionality from randomized measurements. PRX Quantum. 2023;4:020324.
39. Wyderka N, Ketterer A. Probing the geometry of correlation matrices with randomized measurements. PRX Quantum. 2023;4:020325.
40. Liu S, Fadel M, He Q, Huber M, Vitagliano G. Bounding entanglement dimensionality from the covariance matrix. Quantum. 2024;8:1236.
41. Moroder T, Bancal J-D, Liang Y-C, Hofmann M, Gühne O. Device-independent entanglement quantification and related applications. Phys Rev Lett. 2013;111:030501.
42. Brunner N, Pironio S, Acin A, Gisin N, Methot AA, Scarani V. Testing the Hilbert space dimension. Phys Rev Lett. 2008;100:210503.
43. Pal KF, Vertesi T. Efficiency of higher dimensional Hilbert spaces for the violation of Bell inequalities. Phys Rev A. 2008;77:042105.
44. Vertesi T, Pal KF. Bounding the dimension of bipartite quantum systems. Phys Rev A. 2009;79:042106.
45. Pal KF, Vertesi T. Quantum bounds on Bell inequalities. Phys Rev A. 2009;79:022120.
46. Pal KF, Vertesi T. Maximal violation of a bipartite three-setting, two-outcome Bell inequality using infinite-dimensional quantum systems. Phys Rev A. 2010;82:022116.
47. Navascues M, de la Torre G, Vertesi T. Characterization of quantum correlations with local dimension constraints and its device-independent applications. Phys Rev X. 2014;4:011011.
48. de Vicente JI. Shared randomness and device-independent dimension witnessing. Phys Rev A. 2017;95:012340.
49. Le TP, Meroni C, Sturmfels B, Werner RF, Ziegler T. Quantum correlations in the minimal scenario. Quantum. 2023;7:947.
50. Hensen B, et al. Loophole-free Bell inequality violation using electron spins separated by 1.3 kilometres. Nature. 2015;526:682.
51. Giustina M, et al. Significant-loophole-free test of Bell's theorem with entangled photons. Phys Rev Lett. 2015;115:250401.
52. Shalm LK, et al. Strong loophole-free test of local realism. Phys Rev Lett. 2015;115:250402.
53. Rosenfeld W, et al. Event-ready Bell test using entangled atoms simultaneously closing detection and locality loopholes. Phys Rev Lett. 2017;119:010402.
54. Nielsen M, Chuang I. Quantum computation and quantum information. Cambridge: Cambridge University Press; 2010.
55. Batle J, Bednorz A. Null dimension witness based on single measurements. Phys Rev A. 2023;108:062202.
56. Oszmaniec M, Maciejewski FB, Puchała Z. Simulating all quantum measurements using only projective measurements and postselection. Phys Rev A. 2019;100:012351.
57. European Organization for Nuclear Research and Open. AIRE, Zenodo, CERN. 2021. https://doi.org/10.5281/zenodo.8358855.
58. Plaga R. On a possibility to find experimental evidence for the many-worlds interpretation of quantum mechanics. Found Phys. 1997;27:559.
59. Bednorz A. Annalen der Physik. Objective Realism and Joint Measurability in Quantum Many Copies. 2018;530:201800002.